Lidar Atmospheric Measurements on Mars and Earth

C. Dickinson[1], L. Komguem[1], J. A. Whiteway[1†], M. Illnicki[1], V. Popovici[1], W. Junkermann[2], P. Connolly[3], J. Hacker[4]

[1]Department of Earth and Space Science & Engineering, York University, Toronto, ON Canada M3J 1P3
[2]Institut für Meteorologie und Klimaforschung, Forschungszentrum Karlsruhe GmbH
[3]School of Earth, Atmospheric, and Environmental Sciences, University of Manchester, UK
[4]Flinders University and Airborne Research Australia, Adelaide 5001, South Australia
[†]Corresponding Author, (Ph) 001-416-736-2100 x22310, (F) 001-416-736-5189, whiteway@yorku.ca

Keywords – Mars, Phoenix, Lidar, Dust, Aeolian, Cirrus

Abstract

The LIDAR instrument operating from the surface of Mars on the Phoenix Mission measured vertical profiles of atmospheric dust and water ice clouds at temperatures around -65^{o}C. An equivalent lidar system was utilized for measurements in the atmosphere of earth where the conditions are similar to Mars. Coordinated aircraft in situ sampling provided a verification of lidar measurement and analysis methods and also insight for interpretation of lidar derived optical parameters in terms of the dust and cloud microphysical properties. It was found that the vertical distribution of airborne dust above the Australian Desert is quite similar to what is observed in the planetary boundary layer above Mars. Comparison with the in situ sampling is used to demonstrate how the lidar derived optical extinction coefficient is related to the dust particle size distribution. The lidar measurement placed a constraint on the model size distribution that has been used for Mars. Airborne lidar measurements were also conducted to study cirrus clouds that form in the Earths atmosphere at a similar temperature and humidity as the clouds observed with the lidar on Mars. Comparison with the in situ sampling provides a method to derive the cloud ice water content (IWC) from the Mars lidar measurements.

1. Introduction

While the atmospheres of Earth and Mars are significantly different in terms of their molecular composition, several analogies can be made for dust and cloud particles. Dust is lifted into the atmosphere of Mars as in Desert regions on Earth, but since the molecular density on Mars is smaller, the radiative impact of dust is much greater (Wolff et al. 2009). Also, there is a hydrological cycle on Mars that involves clouds and precipitation that form where the temperature and humidity is similar to the conditions in which cirrus clouds form in the upper troposphere on Earth (Whiteway et al. 2009).

The Phoenix Mars mission (Smith et al. 2008, 2009) landed on 25 May 2008, 30 Sols (Martian days) before summer solstice at 68N, 234E. The Lander was operated over the following five months, imaging the surroundings (Smith et al., 2009), digging into the regolith (Shaw et al. 2009), analyzing composition of soil samples (Hecht et al. 2009; Boynton et al. 2009; Kounaves et al. 2009), and measuring atmospheric properties (Taylor et al. 2009, Davy et al. 2009, Tamppari et al. 2009). The lidar instrument on Phoenix (Whiteway et al. 2008) was operated nearly every day during the mission to observe the backscatter of laser radiation from dust, water ice clouds and precipitation in the atmosphere (Whiteway et al. 2009).

The testing and characterization of the Phoenix lidar involved Earth based measurements and direct comparison with an equivalent lidar system (Whiteway et al. 2008). Another aspect of the characterization was field measurements with the equivalent lidar system in conditions that were expected to be similar to Mars. This paper presents case studies where the interpretation of observations on Mars is informed by measurements in the atmosphere of Earth. The insight gained from simultaneous aircraft in situ sampling on Earth is applied for interpretation of the lidar measurements on Mars

2. Mars Phoenix Lidar

The lidar measurement involved emitting a pulse of light into the atmosphere and detecting the light scattered directly back. For earth, the light will be scattered by both molecular constituents and aerosols (dust and ice/water cloud); for Mars, scattering from dust and water ice cloud particles dominate the lidar backscatter signal. The Phoenix lidar is based on a Nd:YAG laser and the frequency doubled output at a wavelength of 532 nm is directed in the zenith. The backscatter is collected by a 10 cm diameter telescope, detected with a Photomultiplier, and the signal is acquired using both analog recording and photon counting. The height resolution after averaging was 20 m for analog recordeing and 50 m for photon counting. The laser was pulsed at a rate of 100Hz, while the acquired profiles were averaged over 2048 pulses for a temporal resolution of 20.48 seconds. The Phoenix lidar was operated typically three times per day with duration between 15 minutes and one hour.

Owing to the greater dynamic range of the analog signals, and the greater sensitivity of the photon counting signals, the choice of whether to use one or both data sets depended on the measured signal strength, or more generally, the proximity of the scatterers to the lidar system. For Phoenix, analog signals below 2.5 km and photon counting data from 2.5 – 20 km were generally used for analysis. Lidar dust measurements from Australia were based entirely on data from the analog channel, while lidar cloud measurements from the EMERALD campaign employed only photon counting

3. Lidar Analysis Method

Figure 1a shows the backscatter signal from Phoenix mission Sol 65 (Solar Longitude, L_S = 106). The signal is from only dust below 8 km, the enhancement above is due to the presence of an ice water cloud. The equation that describes a Lidar backscatter signal as a function of height can be written as $\boldsymbol{S(z) = C \times \beta(z) \times 1/z^2 \times T(z)^2}$. The constant $\boldsymbol{C}$ takes into account factors that include the laser pulse energy, area of the receiver aperture, transmittance of the receiver optics, and the detection efficiency. $\boldsymbol{\beta(z)}$ is the lidar backscatter coefficient and this represents the fraction of optical energy scattered back to the lidar receiver per unit length and per unit solid angle. $\boldsymbol{T(z)}$ is the transmittance through the atmosphere, and is related to the optical depth (OD) as $T(z) = e^{-OD}$ where $OD = \int_0^\infty \sigma dz$. The extinction coefficient, $\boldsymbol{\sigma}$, is the fractional reduction in laser pulse energy per unit length through the atmosphere. It can also be considered the effective cross sectional area of material per unit volume, and is thus proportional to the volume and mass of scattering material.

The backscatter and extinction coefficients, $\boldsymbol{\beta}$ and $\boldsymbol{\sigma}$**,** relate to the properties of material in the atmosphere. These were derived for dust and clouds from the lidar backscatter signal using the method of Fernald (*1984)*, where the inversion requires a reference value at some height. For Mars this reference was obtained by using a value at

2 km that results in a total optical depth from ground to 20 km being matched to the independent measurement made by the Surface Stereo Imager (SSI) instrument (Smith et al. 2008) on Phoenix. For profiles where the presence of ice-water clouds was detected, a background dust profile was first estimated (typically from an adjacent Sol), and it was then assumed that any departure from this baseline was the result of clouds. For Australian dust data, the same method was employed as for Phoenix dust, with the optical depths measured by a CIMEL sun photometer (Qin and Mitchell, 2009) to constrain the results. For the EMERALD data, the reference value was taken below the cloud in the essentially pure molecular atmosphere (with values of $\boldsymbol{\beta}$ and $\boldsymbol{\sigma}$ calculated from nearby radiosonde data). The inversion also requires an assumption on the ratio of extinction to backscatter coefficients (the so called lidar ratio) and values that are typical from earth based measurements were used: 40 for dust (Papayannis *et al.* 2008), and 15 for cloud (Chen, *et al. 2002)*.

Figure 1b shows the vertical profile of extinction coefficient that was derived from the signal in Fig 1a. A layer of enhanced dust loading layer was distributed from the surface up to heights below about 4 km. This is due to the dust that is lifted from the surface and mixed throughout the planetary boundary layer (PBL) by convection and turbulence during daytime. The top of the dust layer corresponds to the top of the PBL. Above 8 km an ice-water cloud is can also be seen.

4. Boundary Layer Dust

The Phoenix equivalent lidar was used for studies of the atmosphere of Earth, emitting the same wavelength of laser light and using identical detectors and data acquisition methods. For Desert dust studies, it was operated from the ground at Muloorina Station in South Australia (29^{o}20'S, 137^{o}90'W, November 11th – 21st, 2007). This is a Desert environment with significant atmospheric dust loading, occasional dust storms, and frequent localized vorticies or *dust devils*. The lidar was observing continuously during the day, while the Dimona aircraft was operated in the area to obtain simultaneous in situ sampling with vertical profiles as well as stacked level flight tracks.

Figure 2 shows profiles of extinction coefficient derived from lidar measurements on Mars from mission sols 14, 48, and 97 (L_S 84°, 99°, and 122°, respectively). The dust loading was greatest around summer solstice in the first 40 sols of the mission and then gradually decreased throughout the remainder of the mission. A profile of lidar extinction measured above the Australian desert on Nov 20th, 2007 at 05:00 GMT is also shown in Fig. 2 for comparison. During heavy dust loading (Sol 14 on Mars and Australia 20 November 2007) the amount of suspended dust and the height of the planetary boundary layer on Earth and Mars are found to be remarkably similar.

Figure 3 shows a contour plot of the dust lidar backscatter coefficient over several hours on 20 Nov. 2007 and the flight altitude of the Dimona Aircraft is indicated with a solid white/black line. The layer of enhanced dust loading grew in height in the morning with the convective boundary layer and reached a maximum of 4 km in the mid afternoon. By the following morning only background dust remained and this cycle repeated.

The regular pattern of vertical structures that extend from ground to near the top of the dust layer indicates the presence of convection overshooting the top of the boundary layer. Figure 4 shows this short term variability for a 20-minute subset of the Australian data (02:10 GMT), and for a 15-minute period on Sol 5 (L_S 79) at the Phoenix site. In both instances, the structure within each cell is highly variable, both vertically, and horizontally (represented by the time it was lofted over the site). On Mars, the high degree of variability was coincident with periods of high dust loading, and after Solstice a quiescent period with reduced dust loading, and thus little or no observable dust dynamics, was prevalent. Intense vortices (dust devils) were also observed near both measurement sites throughout the day (see Ellehoj et al. (2009) for Mars), but for Australia these were less frequent than the features at the top of the boundary layer.

The Dimona aircraft flights provided in situ dust particle measurements that were used to verify the lidar extinction retrieval. An optical particle spectrometer, (Grimm model 1.108), was employed to measure particle number density *in situ*, sizing particles with diameters between 350 nm and 20 μm into 15 size bins with a time resolution of six seconds. The instrument measures particle sizes by recording the amount of scatter perpendicular to the beam of a diode laser operated in the red. Air was drawn through a brass inlet line (length: 50 cm, diameter: 2 mm), and fed into a second inlet with dimensions designed to match the true air speed of the aircraft when travelling at its nominal operating speed at an altitude of 2 km. Inlet airflow was 1.2 L / min, and losses of particles larger than 8 μm from the inlet were corrected according to concurrent readings of an FSSP-100 (Forward Scattering Spectrometer Probe) measuring at one second intervals. The aircraft in situ sampling also included measurements of temperature, pressure, wind velocity and humidity throughout the flights.

The extinction coefficient, $\boldsymbol{\sigma}$, was calculated from the in situ measured size spectrum as: $\sigma = \sum Q_i \cdot \pi R_i^2 \cdot N_i$, where N_i is the number density of particles in the size bin i, centered on radius R_i, and with extinction efficiency Q_i calculated using simple Mie scattering theory for spherical particles (Bohren and Huffman, 1983) at wavelength 532 nm. For Australia, Mie parameters were estimated from the work of Qin and Mitchell (2008) while for Mars, parameters from Wolff *et al.* (2009) were employed.

Figure 5 shows a comparison between lidar and in situ measurements during the aircraft descent at 05:00 GMT on 20 November 2007 (Fig. 3). The dust number density, potential temperature, and humidity, derived from aircraft data, each indicate that the boundary layer was vertically well-mixed at that time. The extinction coefficient determined from lidar measurement is in agreement with that derived from in situ measurements, with the best agreement between methods observed for periods of low variation. In this example, the total dust optical depth estimated from the in situ measurements was found to be 0.526, while the dust optical depth measured by the CIMEL sun photometer (matched by the lidar) was found to be 0.552.

The variability in the dust loading is apparent in the horizontal flight legs. The aircraft executed a series of stacked horizontal flight legs back and forth with descending heights above the lidar at around 03:00 GMT on 20 November 2009 (Fig. 3). Fig 6a illustrates the high degree of variability in dust number density along each horizontal leg. The extinction coefficient was determined (as described above) at the sampling intervals of 2-seconds along the horizontal flight legs, and the mean and its associated standard deviation are shown in Fig. 6b. Two lidar extinction coefficient profiles were derived from ten minute averages corresponding to the first (top) flight leg and one hour later when the aircraft was at the minimum height. The mean in situ extinction values are in good agreement with the lidar measurements when comparing the separate profiles at the start and end of the stacked descent. There was similar agreement between the lidar and in situ measurements during each flight through the campaign and this served as a verification of the lidar measurement and retrieval methods.

Fig 7a illustrates how the measured extinction coefficient represents the balance between particle number and particle cross sectional area. The in situ measurement of the particle size spectrum was averaged between heights 2-3 km from the descent at 05:00 GMT (Figure 3). The contribution to the extinction coefficient from each size bin is also shown, with the integrated extinction size spectrum equal to the average extinction coefficient of 0.13 km^{-1}. As indicated by Figure 5a, this is also nearly equal to that derived from the lidar measurements for this height range (σ = 0.14). The area averaged *Effective Radius* was determined to be 3.4 μm, and despite the order of magnitude differences in particle number over the size spectrum, R_{eff} is mainly representative of the largest particles.

A commonly used model for the dust size distribution on Mars is based on a Gamma Distribution with an effective radius of 1.6 μm, and variance of 0.2 (see Wolff *et al.* 2009 and references therein). Figure 7b shows this particle size distribution along with the calculated contribution to extinction. The amplitude of the spectrum has been adjusted so that the extinction approximates the lidar measurement at a height of 2 km on mission Sol 14 (Fig. 2), with σ = 0.14 km^{-1}, and *OD* = 0.57. In this case the total dust number density can be estimated as 15.7 cm^{-3} by integrating this size distribution from 100 nm to 10 μm. This is remarkably similar to the number density measured above the Australian desert (Figs. 5 and 6).

5. Ice-Water Clouds

On Mars, the Phoenix lidar detected clouds at the top of the atmospheric boundary layer (4-6 km) and at the surface in the early morning hours, near the minimum of the diurnal temperature cycle. Only the clouds at the top of the boundary layer (3 – 6 km) will be considered here. These clouds were observed to form each sol after the atmospheric temperature on Mars started to decrease in mid-summer; starting on sol 80 (L_s = 113) and continuing until the end of the mission (sol 148; L_s = 147). Throughout this period, the cloud base height generally decreased and the clouds persisted later into the day. Figure 8 shows contour plots of the lidar backscatter coefficient from clouds detected over the Phoenix site on mission sols 95 and 99. The base of the cloud on sol 95 exhibits downward extending finger-like structures. This pattern is similar to what is often observed on Earth and has been called *Cirrus Mammatus* (Wang and Sassen 2006), or more commonly *Virga*. The base of the cloud observed on sol 99 after 05:00 has tilted streaks that are also commonly observed in Earth cirrus clouds when wind shear is present. The streaks trace out the motion of ice crystals that form near the cloud top, grow large enough to precipitate hundreds of meters before sublimating in the sub-saturated air below the cloud (Whiteway et al., 2004).

In the time period around sol 95/99 the clouds were observed to form only after 1 AM and this is taken as the time of cloud formation. The ice crystals at the end of the fall streaks on sol 99 would have fallen a distance of 1.5 km over 4 hours. This is consistent with the fall speed in the atmosphere of Mars for an ellipsoidal ice particle having length three times the width and a volume equivalent to a sphere of radius of 35 μm (Fuchs, 1964). This would approximate a columnar ice crystal with width 42 μm and length 127 μm. Such ice crystals are similar to the hexagonal columns that have been sampled in earth cirrus clouds (Whiteway et al. 2004, Gallagher et al. 2005).

The vertical profile of extinction coefficient derived from the average lidar signals on sol 95 is shown in Fig. 9 along with estimated temperature and humidity profiles. The environment in which the clouds form was investigated with a model of the boundary layer on Mars that takes account of the radiative transfer and turbulent mixing (Davy et al. 2009). This made use of the Phoenix lidar observations of dust distribution and the measurements of temperature at the surface. The simulated profiles of temperature at 1

AM and 5 AM on are shown in Fig 9b. Assuming that the cloud ice crystal nucleation commenced at 1 AM, the cloud observed on sol 95 would have commenced formation at a height of about 5.1 km where the temperature of the air was -67.6^{o} C. If the cloud formed when the relative humidity over ice (RH_i) reached a threshold of 100% the vapour pressure would be 0.38 Pa, or a water vapour density of 4.0 mg m^{-3}. Laboratory experiments have found that the threshold for ice nucleation on desert dust is up to RH_i = 130% (Field et al. 2006). The estimate of water vapour density at height 5 km on sol 95 is in then in the range 4 – 5 mg m^{-3}.

A similar analysis was also applied to the sol 99 case by Whiteway et al. (1999). The cloud formed initially at height 4 km where the temperature was -64.5^{o} C and the water vapour density was in the range of 6.2 – 8.0 mg m^{-3}. This corresponds to a volume mixing ratio in the range 0.0012 – 0.0016. The Thermal and Electrical Conductivity Probe on Phoenix measured the partial pressure of water vapour at the surface to have values up to 2 Pa during daytime and less than 0.1 Pa at night with a diurnal average of approximately 0.9 Pa (Zent et al. 2009). The diurnal mean volume mixing ratio at the surface was 0.0012. It can be expected that the mixing ratio within the well mixed boundary layer (up to 4 – 5 km) will be constant away from the surface (as in Fig 5) and equal to or slightly greater than the diurnal mean at the surface. The estimate of water vapour density at the cloud formation height is thus consistent with the measurements at the surface. This temperature and humidity range is similar to the environment in which cirrus clouds form on Earth and it is thus not surprising that the cloud structure observed on Mars is consistent with ice crystals that are similar in size to what has been sampled in Earth cirrus clouds.

The lidar cloud measurements on Mars were compared with combined lidar and aircraft in situ measurements of cirrus above Adelaide Australia during the EMERALD-1 (Egrett Microphysics Experiment with Radiation, Lidar, and Dynamics) field campaign near Adelaide Australia in September 2001 (Whiteway et al. 2004). A lidar system (equivalent to the Phoenix lidar) was viewing upward from one aircraft (King Air), while in situ measurements were carried out within the cirrus clouds from the Egrett aircraft. A Forward Scattering Spectrometer Probe (FSSP) provided the size spectrum of ice crystals in the range of 3 – 40 μm, while the Cloud Particle Imager (CPI) provided imaging of the ice crystals in the size range of 10 – 500 μm (Gallagher et al 2005). Humidity was measured with a cryogenic frost point hygrometer (Busen and Buck, 1995) and Temperature was measured with a Rosemount PT500 sensor.

The Egrett in situ measurements were used to derive the optical extinction coefficient and the Ice Water Content (IWC). The individual images from the CPI were processed and their projected area and length was found. The particle images were corrected for over sizing biases and the sample volume was corrected using a recent calibration method (Connolly et al 2007). The corrected images were classified into habits using the automated habit classification scheme described in table 2 of Baran et al. (2009). The mass-dimension relations of Heymsfield et al. (2002) were used for the particular habit of the classified ice particle images - these are also reproduced in Table 3 of Baran et al

(2009). Finally the CPI data were binned into a time series of IWC and extinction. For the FSSP, particles were assumed to be quasi-spherical and have the density of hexagonal ice (910 kg m-3). In order to calculate extinction we make the assumption that we are in the regime where the size parameter (ratio of the size of the particle to the wavelength of light) is greater than 30. In this regime, one can assume that the extinction is twice the integrated projected area of an ensemble of crystals per unit volume. Hence the extinction coefficient was computed as the sum of the area per unit volume of each crystal from the CPI and each particle from the FSSP (taking into account the overlapping size bins of both probes) and multiplying this by two.

Figure 10 shows the combination of lidar remote sensing and in situ sampling from flights on the 11^{th} and 18^{th} of September, 2001. In each case ice crystals formed at the cloud top where temperatures were below -55 ^{o}C and the air was saturated with water vapour at densities below 10 mg/m^3; conditions similar to those estimated for water ice clouds observed by the lidar on Mars. The extinction coefficients derived from the lidar and in situ probes were found to be in reasonable agreement on each flight (Figure 10d). The horizontal separation of the aircraft was kept within a few kilometers, but it is still difficult to make direct comparisons between the measurements at a specific instant due to the natural variability within the cloud. The average values of the extinction coefficients were 0.40 km^{-1} from the lidar and 0.40 km^{-1} from in situ measurements for the 11 September flight. The agreement was similar on the 18 September flight with 0.15 km^{-1} from the lidar and 0.14 km^{-1} from the in situ measurements.

In situ measurements of Earth cirrus were used to obtain an empirical relationship between the extinction coefficient and the ice water content (IWC), and this relationship was subsequently applied to the measurements on Mars. As the extinction coefficient for water-ice is the effective cross-sectional area per unit volume, it is also related to the mass of ice crystals per unit volume. If the crystals were spherical, the relationship would simply be $IWC = \frac{4}{3} \cdot R_{Eff} \cdot \sigma \cdot \rho_{ICE} \cdot Q^{-1}$, where R_{eff} is the area averaged radius, $\boldsymbol{\sigma}$ is the extinction coefficient, ρ_{ice} is the density of bulk ice (910 kg m^{-3}) and Q is the extinction efficiency for Mie scattering. The ice crystals within a cirrus cloud are actually an ensemble of hexagonal columns and irregular shapes (Whiteway et al 2005; Gallagher et al 2005), so a more accurate representation would be expected from an empirical relationship. As the lidar and in situ extinction coefficients are in general agreement, the IWC–extinction relationship can be obtained from the in situ measurements alone, as this removes any effects due to spatial variability between lidar and in situ measurements. Figure 11 shows the scatter plot of IWC vs. extinction from three flights on 11, 18, and 19 September, 2001. The best linear fit in the range of extinction coefficients observed on Mars (0.01 – 0.2 km^{-1}) is $IWC\,[g/m^3] = 10.0 \cdot \sigma\,[m^{-1}]$. This is slightly different from the result obtained by Heymsfield et al. (2005), but both are within the scatter of the data. The discrepancy could be attributed to differences in the shape of the crystals between the different studies, and in this respect it is an indication of the uncertainty.

The IWC of the cloud observed on sol 95 was estimated by applying the empirical relationship derived from the EMERALD-1 data (Fig. 9d). The ice-water extinction coefficient at height 5.1 km had a value of 0.09 km^{-1} after subtracting the extinction coefficient due to dust. The corresponding estimate of IWC is 0.9 mg m^{-3} by applying the empirical relationship from the EMERALD-1 data. Figure 9d show the vertical profile of IWC estimated from the lidar measurements.

A rough prediction of the IWC can be obtained from the decrease in temperature, due to radiative cooling, between the time that the cloud formed and the time of the measurement. While the air is still cooling, it can be expected that the water vapour pressure within the cloud will remain saturated over ice. It will be assumed again that the cloud commenced forming at 1 AM at a height of 5.1 km. At 5 AM the temperature is -69.4^{o} C at height 5.1 km and this corresponds to a saturated vapour pressure of 0.29 Pa, or a density of 3.1 mg m^{-3}. The decrease from the saturated water vapour density at cloud formation (4 mg m^{-3}) would have been deposited on to ice crystals. The 5 AM cloud IWC at height 4 km is then approximately equal to the 0.9 mg m^{-3} change in vapour density between 1 am and 5 am. Thus the estimate of IWC at 5.1 km from the lidar measurement (0.9 mg m^{-3}) is consistent with the estimate based on changing temperature profile. This calculation was carried out at each height through the cloud to obtain the model IWC profile in Fig. 9c.

6. Conclusions

Lidar measurements of dust from the Australian desert and Mars Phoenix site show several similarities, most notably in the magnitude of the optical extinction coefficients, and the depth of the planetary boundary layers. During periods of high dynamic activity, both sites exhibited analogous structures in the distribution of dust due to convective cells extending above the PBL.

Comparison of aircraft in situ sampling with lidar measurements provides a strong verification for the lidar measurement and analysis methods. Martian dust microphysical properties were derived from lidar extinction profiles with $\sigma = 0.14$ km^{-1}, and an estimate for the average total number density at 2 km was found to be 15.7 cm^{-3}.

Lidar measurements of clouds on Mars were found to exhibit similar structure and optical characteristics to cirrus clouds observed above Adelaide, Australia. Aircraft in situ measurements were used to derive an empirical relationship between optical extinction coefficient and ice water content, and this was applied to the lidar measurements on Mars.

7. Acknowledgements

This work was enabled by funding from the Canadian Space Agency under contract 9F007-070437/001/SR. The Phoenix mission was led by the University of Arizona, on behalf of NASA, and managed by the Jet Propulsion Laboratory. The EMERALD project was funded by the UK Natural Environment Research Council (NERC). The Facility for Ground-based and Atmospheric Measurement (FGAM) provided the CPI instrument during the EMERALD campaign. The Egrett and Dimona aircraft are owned and operated by Airborne Research Australia at Finders University.

8. References

Baran, A. J., Connolly, P. J. , Lee, C. , 2009. Testing an ensemble model of cirrus ice crystals using midlatitude in situ estimates of ice water content, volume extinction coefficient and the total solar optical depth. Journal Of Quantitative Spectroscopy & Radiative Transfer 110 (14-16), 1579-1598.

Bohren, C. F. and Huffman, D. R. , 1983. Absorption and scattering of light by small particles, New York, Wiley.

Boynton, W. V. et al., 2009, Evidence for Calcium Carbonate at the Mars Phoenix Landing Site. Science 325*,* 61-64.

Busen, R., and Buck, A. L., 1995, A high-performance hygrometer for aircraft use: Description, installation and flight data. Journal *of Atmospheric and* Oceanic Technology 12, 73–84.

Chen, W-N., Chiang, C-W. and Nee*,* J-B., 2002. Lidar Ratio and Depolarization Ratio for Cirrus Clouds. Applied Optics 41**,** 6470–6476.

Connolly, P. Et al., 2007. Calibration of the Cloud Particle Imager Probes Using Calibration Beads and Ice Crystal Analogs: The Depth of Field. Journal of Atmospheric and Oceanic Technology 24(11), 1860–1879

Davy, R., et al., 2009. Initial analysis of air temperature and related data from the Phoenix MET station and their use in estimating turbulent heat fluxes. Journal of Geophysical Research, in press.

Ellehoj, M.D. et al., 2009. Convective vortices and Dust Devils at the Phoenix Mars Mission landing site Journal of Geophysical Research - Planets, in press.

Fernald, F.G., 1984. Analysis Of Atmospheric Lidar Observations - Some Comments. Applied Optics, 23(5), 652-653.

Fuchs, N. A., 1964. The Mechanics of Aerosols. Pergamon, New York.

Gallagher, M. W. et al., 2005. An overview of the microphysical structure of cirrus clouds observed during EMERALD-1. Quarterly Journal of the Royal Meteorological Society 131, 1143–1169.

Hecht M. H. et al., 2009. Detection of Perchlorate and the Soluble Chemistry of Martian Soil at the Phoenix Lander Site. Science 325*,* 64-67.

Heymsfield, A. J., et al. 2002. A general approach for deriving the properties of cirrus and stratiform ice cloud particles . Journal Of The Atmospheric Sciences 59(1), 3-29.

Heymsfield, A. J., et al., 2005. Extinction-ice water content-effective radius algorithms for CALIPSO. Geophysical Research. Letters. 32, L10807.

Kounaves, S. M. et al., 2009. The Wet Chemistry Experiments on the 2007 Phoenix Mars Scout Lander Mission: Data Analysis and Results. Journal of Geophysical Research - Planets*,* in press.

Papayannis, A. et al., 2008. Systematic lidar observations of Saharan dust over Europe in the frame of EARLINET Journal of Geophysical Research 113**,** 2000–2002.

Qin, Y. and Mitchell, R. M., 2009. Characterisation of episodic aerosol types over the Australian continent, *Atmos. Chem. Phys., 9*, 1943–1956

Wang L., and Sassen, K., 2006. Cirrus mammatus properties derived from an extended remote sensing dataset. Journal of Atmospheric Science 63, 712 – 725.

Shaw, A. et al., 2009. Phoenix soil physical properties investigation. Journal of Geophysical Research - Planets*,* in press.

Smith, P. H. et al., 2008. Introduction to special section on the Phoenix Mission: Landing Site Characterization Experiments, Mission Overviews, and Expected Science, Journal of Geophysical Research - Planets 113, E00A18.

Smith, P. H. et al*.,* 2009. H_2O at the Phoenix Landing Site. Science 325, 58-61.

Tamppari, L. K. et al., 2009. Phoenix and MRO Coordinated Atmospheric Measurements, Journal of Geophysical Research - Planets*,* in press.

Taylor et al., 2009. Temperature, pressure, and wind instrumentation in the Phoenix meteorological package, Journal of Geophysical Research - Planets *113*, E00A10.

Whiteway, J. et al., 2004. Anatomy of cirrus clouds: Results from the Emerald airborne campaigns, Geophysical Research Letters 31, L24102.

Whiteway, J. et al., 2008. Lidar on the Phoenix mission to Mars. Journal of Geophysical Research - Planets 113, E00A08.

Whiteway, J. et al., 2009. Mars Water-Ice Clouds and Precipitation. Science, 325*,* 68-70.

Wolff, M. J. et al., 2009. Wavelength dependence of dust aerosol single scattering albedo as observed by the Compact Reconnaissance Imaging Spectrometer. Journal of Geophysical Research - Planets, 114, E00D04.

Zent, A.P. et al., 2009. Initial Results from the Thermal and Electrical Conductivity Probe (TECP) on Phoenix. Journal of Geophysical Research - Planets, in press.

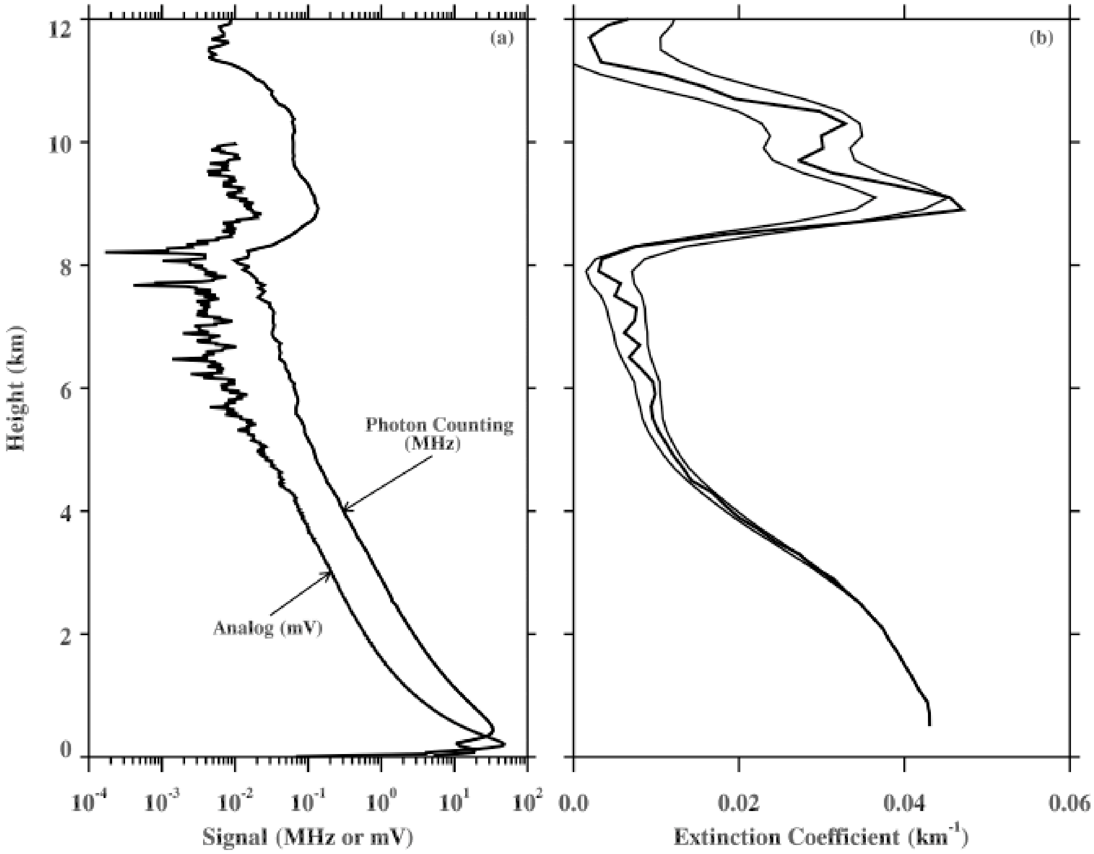

Figure 1. (a) Lidar backscatter signal for both the Analog (milliVolts) and Photon Counting (MHz) on Sol 65, 07:11 Local True Solar Time (L_S = 106^o). (b) Derived extinction coefficient profile for Sol 65 using a lidar ratio of 40. The Analog signal was employed from ground to 2.5 km, and Photon Counting signal from 2.5 – 20km. Relative uncertainty is provided for the extinction coefficient.

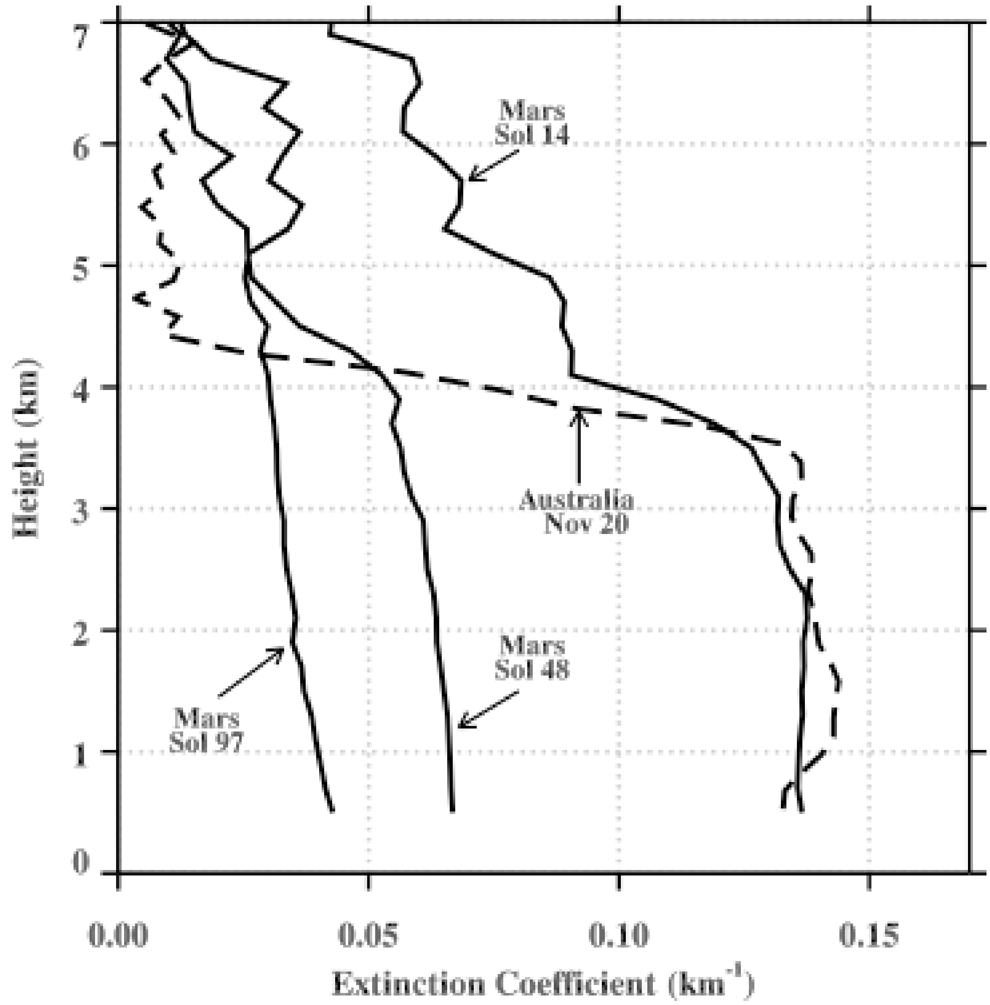

Figure 2. Lidar extinction coefficient profiles for Mars Sols 14, 48, 97 (solid) and at Muloorina Australia on Nov 20th 05:00 GMT (dashed). The solar longitudes of Mars on these dates were $L_s = 84^o$, 99^o, and 122^o.

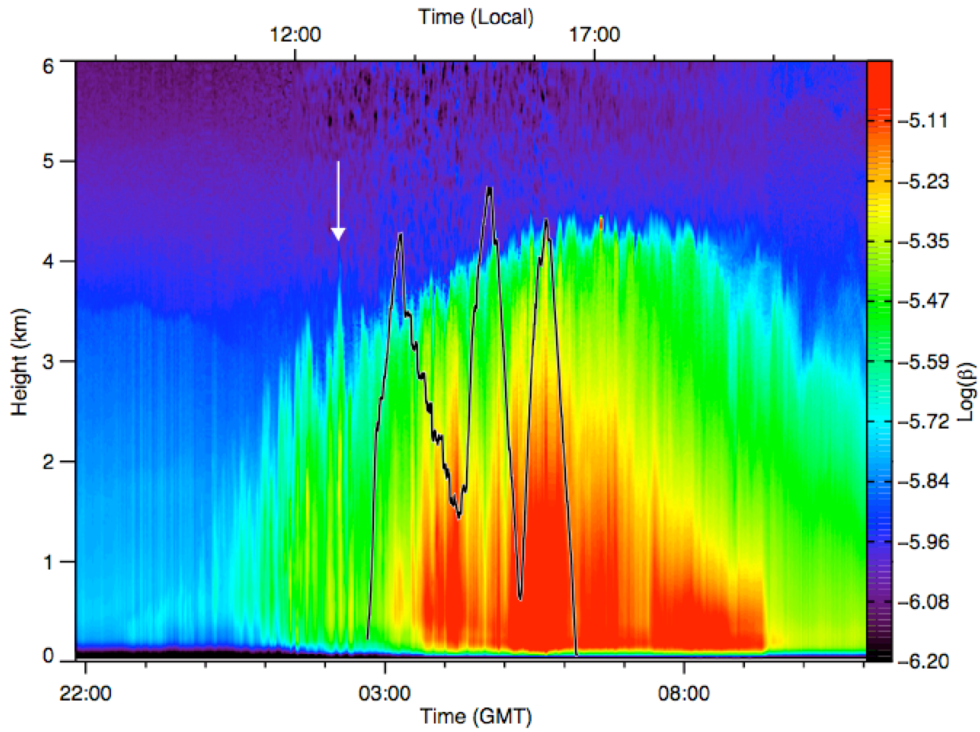

Figure 3. Lidar backscatter coefficient derived from the measurements on November 20th at Muloorina Australia. The solid black line indicates the height of the Dimona aircraft.

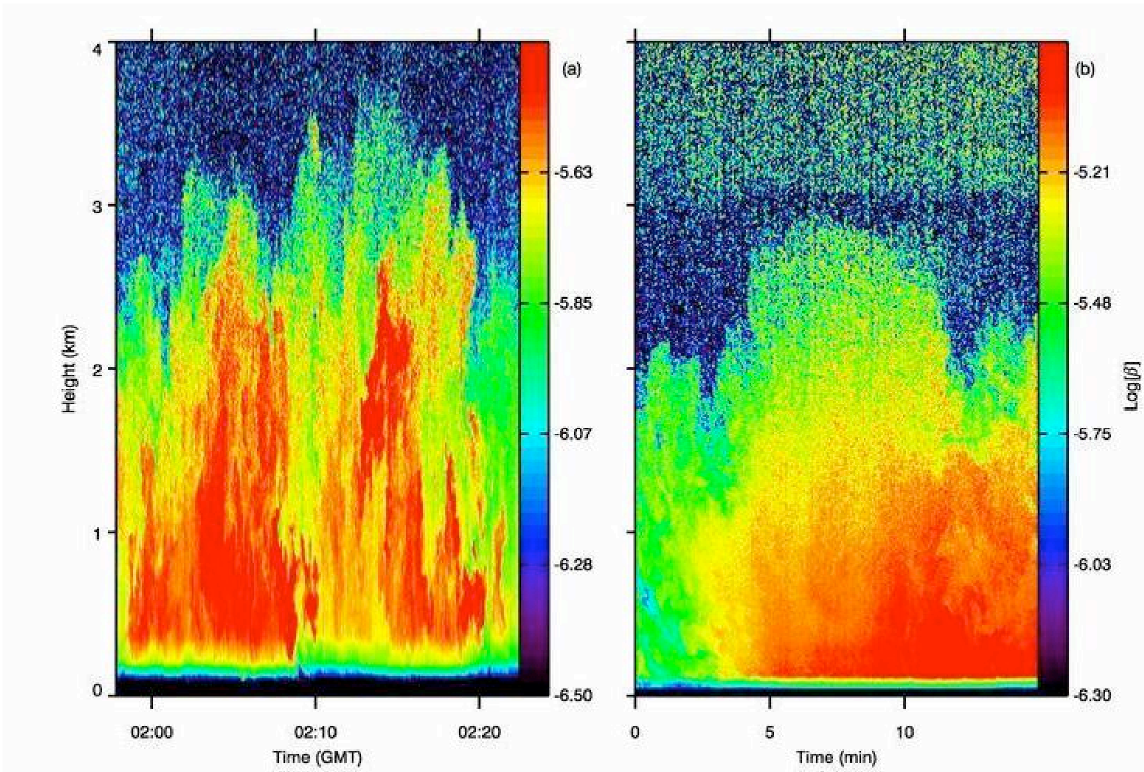

Figure 4. Contour plot of lidar backscatter coefficient over short time periods for (a) November 20th, 03:00 GMT at Australia, and (b) Sol 5 ($L_s = 79^o$) at the Phoenix Mars site (11:00 Local True Solar Time). Both plots are given as LOG(β). Although the structures appear similar, the total dust loading for these examples was observed to be quite different: *OD* = 0.22 and 0.86 for Australia and Mars respectively.

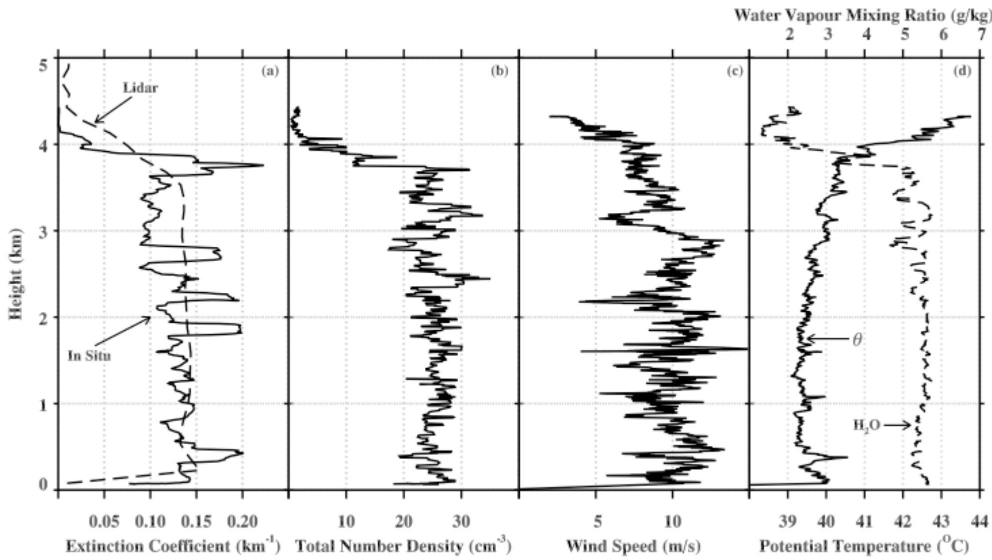

Figure 5. (a) Optical extinction coefficient profiles derived from in situ (solid) and lidar (dashed) measurements on Nov 20th 05:00 GMT. Aircraft in situ measurements of (b) dust number density, (c) wind speed, (d) potential temperature (solid), and (d) water vapour density (dashed). The near vertical profile below 4km in each of these plots illustrates that the PBL was well mixed at this time of day (15:30 Local).

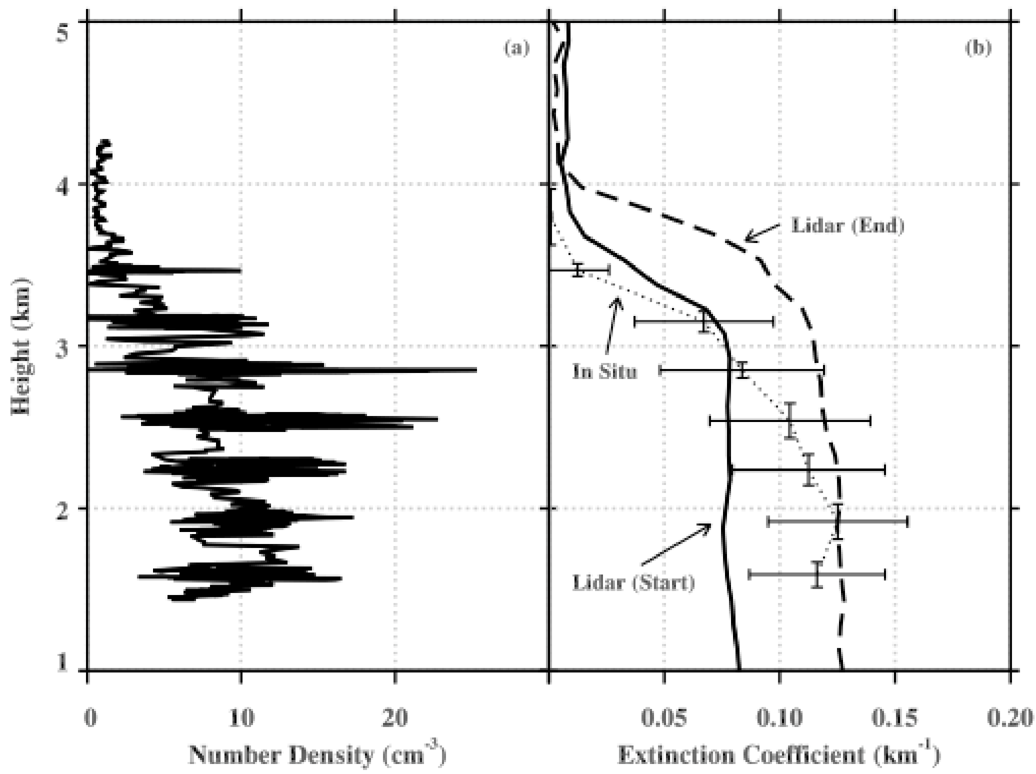

Figure 6. (a) In situ measurements of particle number density. (b) Lidar extinction coefficient profiles at start (solid) and end (dashed) of the aircraft descent. The average extinction coefficients, and associated 1σ standard deviations, were calculated for each horizontal flight leg (crosses), with the dotted line representing the average extinction profile as measured by the aircraft over its one hour descent.

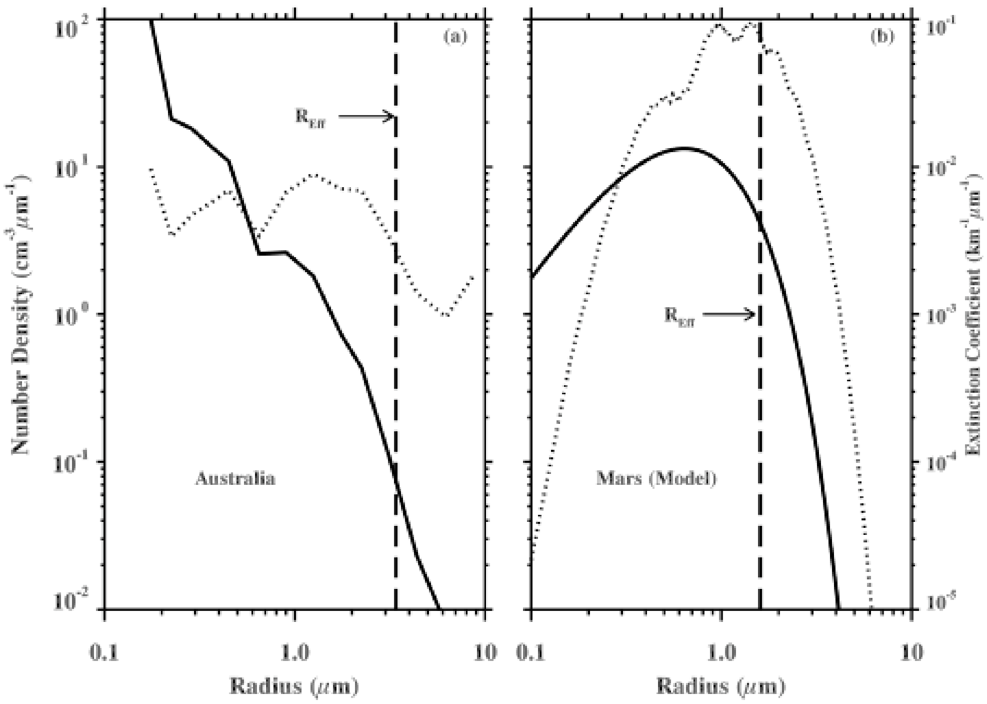

Figure 7. (a) The measured spectrum of particle number density and optical extinction coefficient as a function of particle size from the flight on 20 November, between 2 and 3 km. (b) The model spectrum of particle number density and optical extinction normalized to match the lidar measurement on Mars, Sol 14 ($L_s = 84^o$) at height 2 km. For each plot the *Effective Radius* (R_{Eff}) is given as a dashed vertical line.

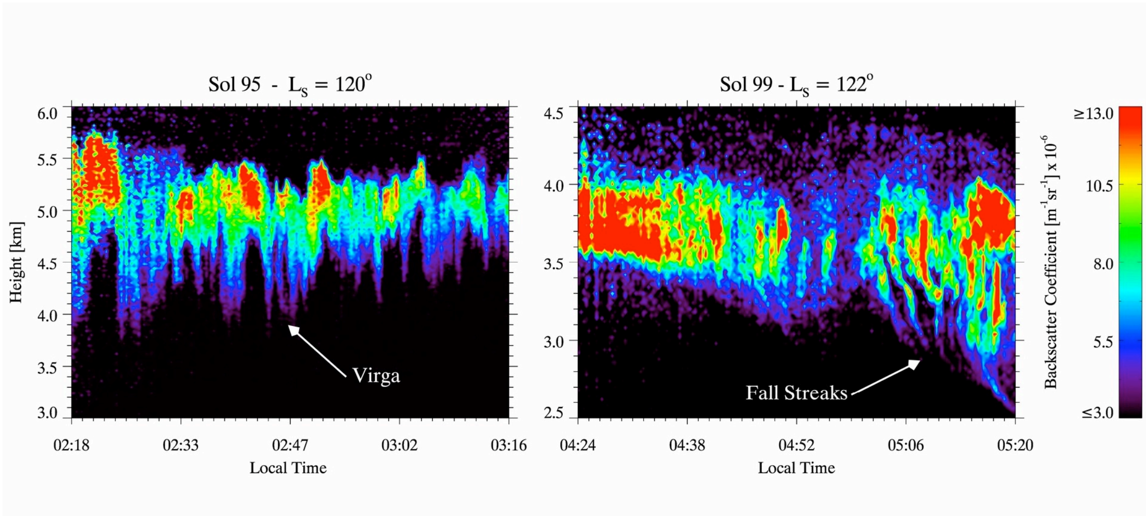

Figure 8. Two case studies of lidar cloud measurements on Mars. Each shows the height distribution of backscatter coefficient over a one hour interval. The colored area is the outline of a cloud that drifted above the landing site. Left: The base of the cloud is deformed into vertical finger-like structures that are caused by precipitating ice crystals that sublimate into the air below the cloud (Virga). Right: The fall streaks are where precipitating ice crystals are stretched out somewhat in the horizontal by wind shear.

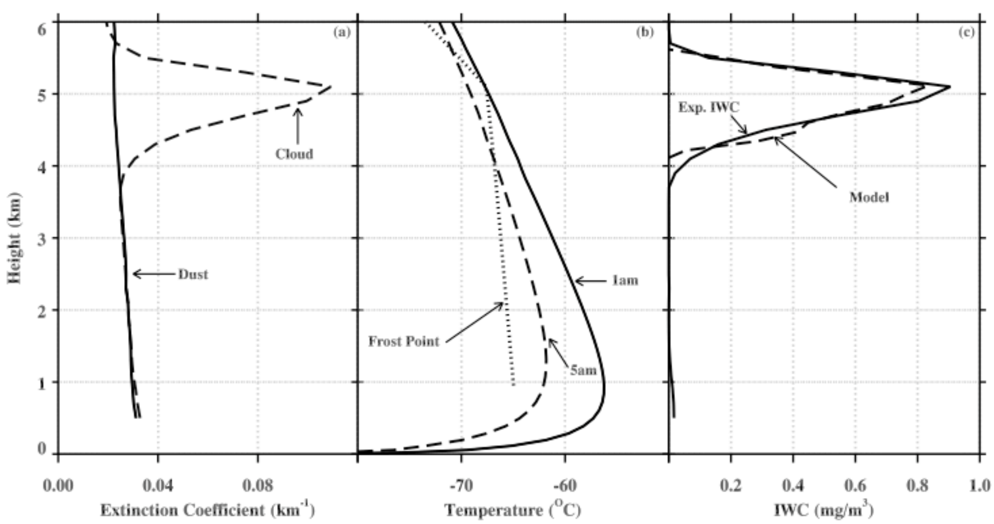

Figure 9. (a) Extinction Coefficient Profile for Sol 95 (L_S = 120) for dust only (solid) and for dust + cloud (dashed). (b) Modeled temperature profiles for 1 am (solid) and 5 am (dashed) on Sol 95. The Frost point (dotted) was estimated from the cloud peak at 1am, constant water vapour mixing ratio below, and intersecting the cloud top temperature above. (c) Derived Ice Water Content from the lidar cloud extinction (solid) and from the modeled 5 am and Frost Point Temperature Profiles of (b) (dashed).

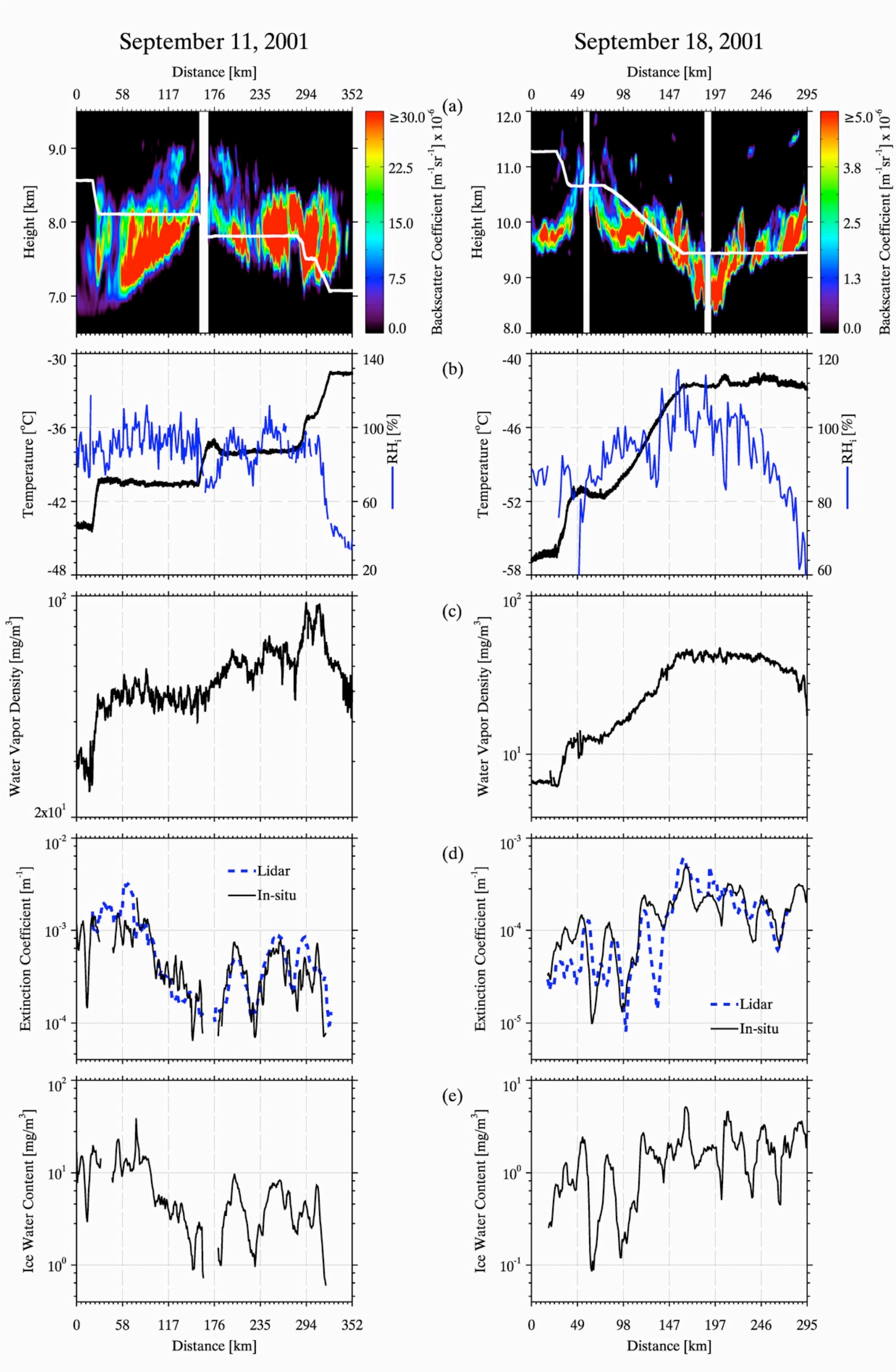

September 11, 2001
September 18, 2001
Distance [km]
Height [km]
Backscatter Coefficient [m⁻¹sr⁻¹] x 10⁻⁶
(a)
(b)
(c)
(d)
(e)
Temperature [°C]
RH_i [%]
Water Vapor Density [mg/m³]
Extinction Coefficient [m⁻¹]
Lidar
In-situ
Ice Water Content [mg/m³]

Figure 10 (a) Airborn lidar measurments of cirrus clouds near Adelaide Australia, on the 11th and 18th of September 2001. The height of the Egrett aircraft and in situ measurements, is given as a white line. Measurements along the Egrett flight path of (b) temperature and relative humidity, (c) water vapour density, (d) derived extinction coefficients, and (e) ice water content calculated from in situ measurements.

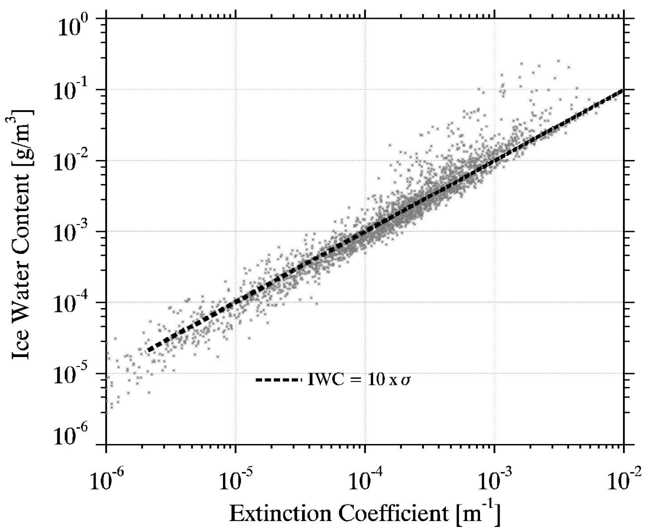

Figure 11. Scatter plot of Ice Water Content versus derived in situ extinction coefficient.